Novel Rotary Encoder with Multi-Axis Hall Sensors

Bruno Brajon[1], Christian Schott[1], and Gaël Close[1]

[1]Affiliation not available

November 28, 2023

Abstract

We present a novel high-accuracy rotary magnetic sensor system composed of a two-track coded multi-pole magnet and a dual-spot multi-axes magnetic sensor. The novelty is the measurement of two orthogonal magnetic field components in each of the two sensing spots of the sensor, one associated with each magnet track. As the two orthogonal signals in each spot are naturally in quadrature, i.e. they represent a sine and a cosine signal, the measurement principle is virtually independent of the magnet pole size and pitch. We can therefore design a magnet with much larger poles which in turn generate stronger magnetic flux, allowing for an increased air gap between sensor and magnet. The calibrated encoder system was characterized to deliver 13 bits of absolute accuracy and 17 bits of resolution over the full 360° range.

Novel rotary Encoder with multi-axis Hall Sensors

Bruno Brajon
Melexis Technologies SA
Bevaix, Switzerland
bur@melexis.com

Christian Schott
Melexis Technologies SA
Bevaix, Switzerland
csc@melexis.com

Gaël Close
Melexis Technologies SA
Bevaix, Switzerland
gcl@melexis.com

***Abstract*—We present a novel high-accuracy rotary magnetic sensor system composed of a two-track coded multi-pole magnet and a dual-spot multi-axes magnetic sensor. The novelty is the measurement of two orthogonal magnetic field components in each of the two sensing spots of the sensor, one associated with each magnet track. As the two orthogonal signals in each spot are naturally in quadrature, i.e. they represent a sine and a cosine signal, the measurement principle is virtually independent of the magnet pole size and pitch. We can therefore design a magnet with much larger poles which in turn generate stronger magnetic flux, allowing for an increased air gap between sensor and magnet. The calibrated encoder system was characterized to deliver 13 bits of absolute accuracy and 17 bits of resolution over the full 360° range.**

***Index Terms*—Encoder, Magnet, Vernier, Nonius, Multipole, Off-axis**

I. Introduction

Absolute angular encoders are widely spread in industrial applications with the robotic market as an important emerging segment [1]. Contactless rotary position sensing is dominated today by three distinct technologies: optical, magnetic and inductive [Table I]. Optical encoders are well known to deliver overall accuracy of up to 16 bits and resolution to over 20 bits due to the implementation of many tracks with very fine structures [2]. However, as they are error-prone to contamination by dust particles, droplets etc, the encoders must be hermetically sealed which makes them bulky and expensive [3]. Inductive encoders yield similar resolution and accuracy, however they require large area for good coupling and full circular PCB for through-shaft applications [4]. Magnetic encoders on the other hand come in many flavors today. from the simple end-of-shaft components with dipole magnets [5] to circular magnetic scales with several pole pairs along the perimeter [6]. This is an ideal concept to map a rotary angle of 360 electrical degrees to a mechanical angle of 360°/*n* and so to increase resolution and accuracy by a factor of *n*. For the sensing of such a track, a small sensor chip having two or more sensing elements within a few millimeters distance is typically used [7]. The sensing elements are integrated horizontal Hall devices measuring the field component perpendicular to the chip surface. Two sensing elements per track are spaced at a distance corresponding to half a pole length and thus generate a sine and a cosine signal through which the angular position with the pole-pair is calculated. This fixed distance restricts the system use to a single pole pitch and very small radial misalignment causes significant orthogonality errors which require compensation [8]. By combining two magnetic scales into a Vernier configuration where a Master track with n pole pairs and a Nonius track with $n-1$ pole pairs are used, the magnet is made asymmetric and true 360° measurement capability is enabled [9]. Due to the small distance between the sensing elements on the integrated chip, the poles of the magnetic scale are typically between 1 and 2mm long [10] and the sensor chip operates at a distance of 0.5 to 1mm from the magnetic scale surface. If a single-track magnetic scale with coded poles is used then the poles are even smaller and consequently the air gap further reduced [11]. This requires very accurate mechanical adjustment of the sensor and magnet and it bears the risk of destruction of the magnetic scale by mechanical contact with the sensor if slightly misaligned. In our approach, we intentionally break the link between sensing element distance and pole size by introducing multi-axis sensing enabled by 3D Hall magnetic field sensors.

TABLE I
Encoder Benchmark

Device	Technology	Accuracy	Resolution*	Power
[5]	Magnetic	10 bit	14 bit	50 mW
[7]	Magnetic	12 bit	18 bit	265 mW
[4]	Inductive	15 bit	20 bit	425 mW
[12]	Optical	14.5 bit	23 bit	650 mW
[11]	Magnetic	14 bit	19 bit	650 mW
This work	Magnetic	13 bit	17 bit	100 mW

*Resolution is the RMS noise in a bandwidth of 500 Hz

II. Sensing concept

A. Single sensing spot per track

Instead of using two sensing spots per track measuring the same component of the magnetic field in two separate locations, we use a single sensing spot measuring two orthogonal magnetic field components e.g. one axial B_a and one tangential B_t [Fig.1]. With an appropriate magnet design where the axial component has a sine shape and the radial component is about zero, the tangential component automatically shows the behavior of a cosine function when the magnet rotates.

B. The link between pole size, air-gap and tolerances

The "single spot - two components" feature allows the use of the same sensing device in combination with a large range of magnet pole sizes. We can therefore work with pole dimensions that are significantly larger than the sensor chip. Bigger poles are naturally stronger so that we can increase the distance between the magnetic scale and the sensor significantly. Using a 24mm diameter magnetic scale with 8 pole pairs where each pole is more than 4mm long, we work with a nominal air gap of 2mm. A larger air gap bears two distinct advantages:

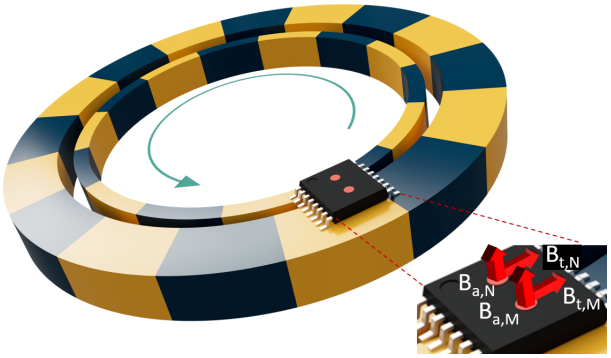

Fig. 1. Encoder consisting of a dual-track multi-pole Magnet and a dual-spot multi-axis magnetic field sensor

- The change of the air gap with temperature or with lifetime wear-out has a relatively smaller impact on measured magnetic field components
- The mutual positioning of the magnetic scale and the sensor chip allows for much larger assembly tolerances.

III. From Magnet to Angle

In this concept, the four signals measured by the sensor are:

$$B_{\mathrm{t,M}} = B_{\mathrm{m}} \cos 8\phi + c_1 B_{\mathrm{n}} \cos 7\phi \quad (1)$$

$$B_{\mathrm{a,M}} = B_{\mathrm{m}}(1+\alpha_1) \sin(8\phi + \theta_1) + c_2 B_{\mathrm{n}} \sin(7\phi + \theta_2) \quad (2)$$

$$B_{\mathrm{t,N}} = B_{\mathrm{n}} \cos 7\phi + c_3 B_{\mathrm{m}} \cos 8\phi \quad (3)$$

$$B_{\mathrm{a,N}} = B_{\mathrm{n}}(1+\alpha_2) \sin(7\phi + \theta_2) + c_4 B_{\mathrm{m}} \sin(8\phi + \theta_1) \quad (4)$$

where ϕ is the mechanical rotation angle, B_{m} and B_{n} are the field amplitudes of the Master and the Nonius track, α_1 and α_2 describe the amplitude mismatch, θ_1 and θ_2 the phase mismatch and c_1, c_2, c_3, c_4 denote the cross-talk between the two magnetic tracks. On top of this, we observe errors arising from magnet imperfections like inaccurate pole separations and non-homogeneous magnetization. In the following sections, we will guide the reader by a step-wise approach to how each of those effects is compensated [Fig.3]. The data used in those steps had prior been generated by a referenced calibration, i.e. registering the four sensor outputs versus a high-accuracy reference system.

A. Nonius angle reconstruction

As the Nonius track is very weak, the sensor measuring its components suffers from heavy crosstalk from the strong Master track. Therefore, it is required to reconstitute the Nonius signal by a linear combination of all four sensor signals.

$$\tilde{B}_{\mathrm{a,N}} = d_1 B_{\mathrm{t,M}} + d_2 B_{\mathrm{a,M}} + d_3 B_{\mathrm{t,N}} + d_4 B_{\mathrm{a,N}} \quad (5)$$

$$\tilde{B}_{\mathrm{t,N}} = d_5 B_{\mathrm{t,M}} + d_6 B_{\mathrm{a,M}} + d_7 B_{\mathrm{t,N}} + d_8 B_{\mathrm{a,N}} \quad (6)$$

where $d_1, ..., d_8$ are coefficients that have been extracted during the calibration procedure by a least square fit. $\tilde{B}_{\mathrm{a,N}}$ and $\tilde{B}_{\mathrm{t,N}}$ are the reconstructed Nonius signals. We can now extract the Nonius angle:

$$7\phi_{\mathrm{LC}} = \arctan\left(\frac{\tilde{B}_{\mathrm{a,N}}}{\tilde{B}_{\mathrm{t,N}}}\right) \quad (7)$$

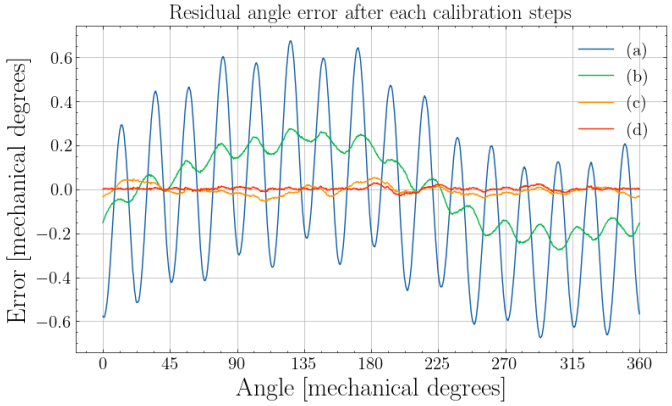

Fig. 2. (a) shows an error of $\pm 0.067°$ containing a dominant component with 16 periods.(b) shows an error of $\pm 0.28°$ and dominant components with one and 15 periods.(c) shows a residual harmonic error of $\pm 0.055°$. (d) shows the residual error after calibration ($\pm 0.015°$)

$7\phi_{\mathrm{LC}}$ is required to assign a unique sector number ranging from 0 to 7 to each pole pair of the Master track, making the system a true power-on absolute encoder.

B. Amplitude and Phase Correction

In this step, we match the amplitude and the phase for the Master source signals. Such mismatch causes the presence of a 16^{th} harmonic in the error [Fig. 2(a)]. The following equation shows the correction function that needs to be applied to $B_{\mathrm{a,M}}$ [13]:

$$\tilde{\tilde{B}}_{\mathrm{a,M}} = \frac{(A_0 B_{\mathrm{a,M}} + (\sin A_1) B_{\mathrm{t,M}})}{\cos A_1} \quad (8)$$

A_0 and A_1 are the coefficients compensating for amplitude and phase mismatching. They are determined during the calibration procedure by solving a least square problem minimizing the 16^{th} harmonic content in the angle error.

C. Fine angle reconstruction

After the amplitude and phase correction, equations (1) and (2) are written as follows:

$$B_{\mathrm{t,M}} = B_{\mathrm{m}}(\cos(8\phi) + k_1 \cos(7\phi)) \quad (9)$$

$$\tilde{\tilde{B}}_{\mathrm{a,M}} = B_{\mathrm{m}}(\sin(8\phi) + k_2 \sin(7\phi)) \quad (10)$$

The main error contribution is the crosstalk between the Master track and the Nonius track which will be treated in section III-D. We can now extract the angle from the Master track signals:

$$8\phi_{\mathrm{ct}} = \arctan\left(\frac{\tilde{\tilde{B}}_{\mathrm{a,M}}}{B_{\mathrm{t,M}}}\right) = 8\phi + \epsilon_{\mathrm{ct}} \quad (11)$$

where ϵ_{ct} is the angular error due to the crosstalk. The mechanical angle is retrieved by the following expression:

$$\phi_{\mathrm{mech}} = 8\phi_{\mathrm{ct}} - 7\phi_{\mathrm{LC}} = \phi + \epsilon_{\mathrm{coarse}} \quad (12)$$

$\epsilon_{\mathrm{coarse}}$ is the error in the discrimination of the Master sector. Since we are using 8 pole pairs this error needs to be lower than $\pm 22.5°$. Using ϕ_{mech}, we are able to assign to each

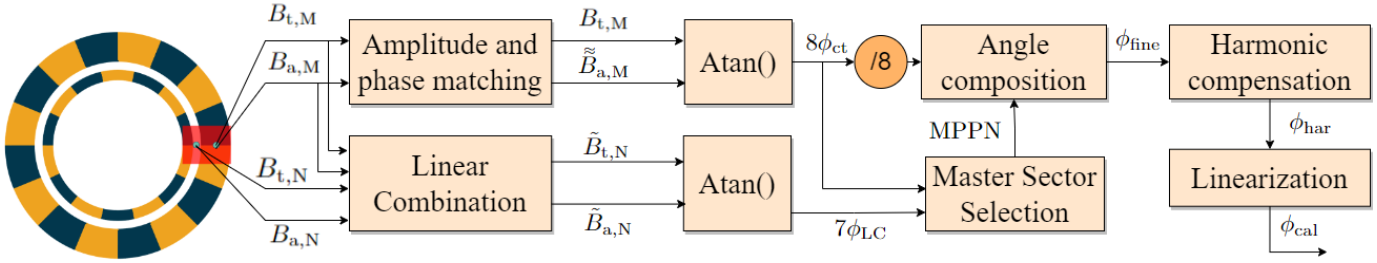

Fig. 3. The signal flow from magnet to angle

Master pole pair a unique Master Pole Pair Number (MPPN) from 0 to 7. At this point, we are able to extract the fine angle which will be equal to :

$$\phi_{\text{fine}} = \text{MPPN} \times 45° + (8\phi_{\text{ct}} \mod 360°)/8 = \phi + \epsilon_{\text{ct}}/8 \tag{13}$$

We recognize that in (13) the error of the angle measured is reduced by a factor 8.

D. Harmonic correction and linearization

After dealing with the Amplitude and Phase mismatching, we address the challenge arising from cross-talk between Master and Nonius magnet due to their close distance. After some mathematical manipulations, we can express the angle error due to cross-talk for the Master track as:

$$\epsilon_{\text{ct}} = (k_1 + k_2)\sin(\phi)/2 + (k_1 - k_2)\sin(15\phi)/2 \tag{14}$$

This equation is valid if $k_1, k_2 \ll 1$.

We can identify in (14) the presence of a 1^{st} harmonic and a 15^{th} harmonic in the error curve. In experimental data, we measured $k_1 = 2\%$ and $k_2 = 3\%$ and we observe these harmonics in Figure 2(b). To reduce the contribution of these harmonics we need to solve a minimization problem in the form of :

$$\phi_{\text{har}} = \phi_{\text{fine}} - \sum_{h\in\{1,15\}} j_h \sin(h\phi_{\text{fine}} + p_h) \tag{15}$$

After finding the coefficients j_h and p_h we are left with the non-linearity due to the imperfections of the magnet [Fig.2(c)]. To compensate for this we use a Look-Up-Table (LUT) to store the reference angle information for certain measured angle positions. Then the corrective value is found through interpolation of the LUT points according to the measured position[Fig.2(d)].

$$\phi_{\text{cal}} = \phi_{\text{har}} - f_{\text{LUT}}(\phi_{\text{har}}) \tag{16}$$

IV. Realization of the Novel Rotary Encoder

The realized encoder prototype is shown in Fig. 4. The sensor chip contains two configurable 3-axis magnetic field sensor devices assembled together side-by-side inside a TSSOP16 package. The distance between the sensitive spots of the two dies is 1.9mm. The sensor chip is mounted on a PCB and fixed at a 2mm distance from the magnetic scale surface. The magnetic scale with two tracks, a first external Master track with 8 pole pairs and a second internal Nonius track with 7 pole pairs. Its outside diameter is 24mm with an inner through-shaft opening of 14mm. The scale is mounted on the axis of a commercial stepping motor with reduction gear. We use a separate high-accuracy magnetic sensor with its own magnet and sensor chip as a reference encoder [11]. Both systems are calibrated after assembly to eliminate the impact of manufacturing and assembly tolerances on the angle position output. The angular performance is assessed by the output difference between our system and the reference system with the motor stepping through the full 360° circle. As shown in [Fig.2(d)], this difference is lower than $\pm 0.03°$ over the full magnet rotation. The amplitude of the magnetic field captured at a 2mm distance is large enough to deliver 18-bit RMS resolution for 1 ms integration time.

V. Conclusion

In this paper, we explain and demonstrate a novel high-accuracy sensing concept based on a multi-axis magnetic sensor combined with a novel dual-track magnet with large and thus strong magnetic poles. With a 2mm nominal air gap between sensor and magnet the system outperforms the current state of the art technologies on the initial placement tolerances and on lifetime wear-out. The system accuracy is better than 0.03° over the full 360° rotation. This angular encoder is a general-purpose sensing device and may be used in a broad range of angle positioning and motor driver applications.

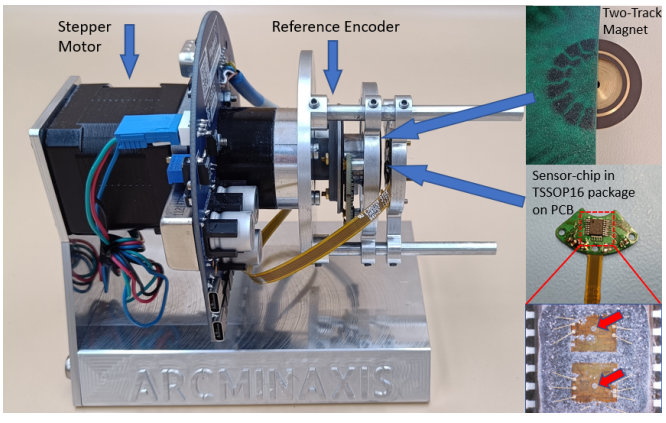

Fig. 4. Demonstrator and Test Setup of the Novel Rotary Encoder. Insert Pictures from top: Dual Track Magnet, Sensor on PCB and opened Sensor Die with dual sensitive Spots

REFERENCES

[1] T. Reininger, F. Welker, and M. von Zeppelin, "Sensors in position control applications for industrial automation," *Sensors and Actuators A: Physical*, vol. 129, no. 1, pp. 270–274, 2006, eMSA 2004. [Online]. Available: https://www.sciencedirect.com/science/article/pii/S0924424706000665

[2] DR. JOHANNES HEIDENHAIN GmbH, "Rotary Encoders Catalog." [Online]. Available: https://www.heidenhain.com/fileadmin/pdf/en/01_Products/Prospekte/PR_Rotary_Encoders_ID349529_en.pdf

[3] S. Hao, Y. Liu, and M. Hao, "Study on a novel absolute magnetic encoder," in *2008 IEEE International Conference on Robotics and Biomimetics*, Feb. 2009, pp. 1773–1776.

[4] DR. JOHANNES HEIDENHAIN GmbH, "KCI 120 Dplus." [Online]. Available: https://www.heidenhain.com/products/rotary-encoders/internal/kci-120-dplus

[5] Melexis, "MLX90372." [Online]. Available: https://media.melexis.com/-/media/files/documents/datasheets/mlx90372-datasheet-melexis.pdf

[6] K. Miyashita, T. Takahashi, and M. Yamanaka, "Features of a magnetic rotary encoder," *IEEE Transactions on Magnetics*, vol. 23, no. 5, pp. 2182–2184, 1987.

[7] IC-Haus, "iC-MU MAGNETIC OFF-AXIS POSITION ENCODER POLE WIDTH 1.28MM." [Online]. Available: https://www.ichaus.de/upload/pdf/MU_datasheet_F2en.pdf

[8] T. H. Nguyen, H. X. Nguyen, T. N.-C. Tran, J. W. Park, K. M. Le, V. Q. Nguyen, and J. W. Jeon, "An effective method to improve the accuracy of a Vernier-Type absolute magnetic encoder," *IEEE Trans. Ind. Electron.*, vol. 68, no. 8, pp. 7330–7340, Aug. 2021.

[9] G. V. Prokofiev, V. G. Stakhin, V. V. Misevich, B. L. Krivtz, and M. A. Kosolapov, "Development of a specialized microcircuit for a magnetic precision position sensor based on multipolar magnetic technology."

[10] BOGEN magnetics GmbH, "220530_RMSN_technical_data_sheet." [Online]. Available: https://www.bogen-magnetics.com/media/261/d-1/t-file/220530_RMSN_technical_data_sheet.pdf

[11] RLS, "MBD039." [Online]. Available: https://www.rls.si/eng/aksim-2-off-axis-rotary-absolute-encoder

[12] DR. JOHANNES HEIDENHAIN GmbH, "ROC 1023." [Online]. Available: https://www.heidenhain.com/products/rotary-encoders/external/roc/roq-1000

[13] Z. Gao, B. Zhou, B. Hou, C. Li, Q. Wei, and R. Zhang, "Self-Calibration of nonlinear signal model for angular position sensors by Model-Based automatic search algorithm," *Sensors*, vol. 19, no. 12, Jun. 2019.